Two-temperature hydrodynamics of laser-generated ultrashort shock waves in elasto-plastic solids

2014 J. Phys.: Conf. Ser. 500 032021

(http://iopscience.iop.org/1742-6596/500/3/032021)

Journal of Physics: Conference Series **500** (2014) 032021 doi:10.1088/1742-6596/500/3/032021

Two-temperature hydrodynamics of laser-generated ultrashort shock waves in elasto-plastic solids

Denis K Ilnitsky[1], **Viktor A Khokhlov**[2], **Nail A Inogamov**[2], **Vasily V Zhakhovsky**[3], **Yurii V Petrov**[2], **Konstantin V Khishchenko**[3], **Kirill P Migdal**[1] **and Sergey I Anisimov**[2]

[1] All-Russia Research Institute of Automatics, Rosatom, Moscow, Russian Federation
[2] Landau Institute for Theoretical Physics, Russian Academy of Sciences, Russian Federation
[3] Joint Institute for High Temperatures of Russian Academy of Sciences, Russian Federation

E-mail: nailinogamov@gmail.com

Abstract. Shock-wave generation by ultrashort laser pulses opens new doors for study of hidden processes in materials happened at an atomic-scale spatiotemporal scales. The poorly explored mechanism of shock generation is started from a short-living two-temperature (2T) state of solid in a thin surface layer where laser energy is deposited. Such 2T state represents a highly non-equilibrium warm dense matter having cold ions and hot electrons with temperatures of 1–2 orders of magnitude higher than the melting point. Here for the first time we present results obtained by our new hybrid hydrodynamics code combining detailed description of 2T states with a model of elasticity together with a wide-range equation of state of solid. New hydro-code has higher accuracy in the 2T stage than molecular dynamics method, because it includes electron related phenomena including thermal conduction, electron-ion collisions and energy transfer, and electron pressure. From the other hand the new code significantly improves our previous version of 2T hydrodynamics model, because now it is capable of reproducing the elastic compression waves, which may have an imprint of supersonic melting like as in MD simulations. With help of the new code we have solved a difficult problem of thermal and dynamic coupling of a molten layer with an uniaxially compressed elastic solid. This approach allows us to describe the recent femtosecond laser experiments.

1. Introduction

Shock compression of solids was being studied intensively last several decades [1]. Hugoniot Elastic Limit (HEL) is a key concept in this branch of science. Above the HEL uniaxially deformed state becomes impossible - instead, isotropization of stresses and deformations takes place. For such metals as aluminum, nickel, and so on, the usual values of HEL are small - this means that an elastic shock wave (SW) driven by piston at a stress near HEL has velocity D_{el} only $1-2\%$ higher than elastic sound speed c_{el}. Until recently, before works [2–6], the elastic branch of Hugoniot was widely accepted as a linear function for stresses below the common HEL. This is why a strong elastic SW firstly observed in the excellent pump-probe experiments with femtosecond lasers done by Evans *et al.* [7] and Gahagan *et al.* [8] was not recognized as an elastic wave. Such an elastic SW moves with velocity notably higher the longitudinal sound speed, and notably faster than the plastic SW with the same amplitude of pressure. Estimating those papers we can say today that they were well ahead of their time. Recent calculations [9] show that in the experiments [7] degree of nonlinearity of elastic SW was significant $D_{el}/c_{el}-1 \approx 0.1-0.2$. In

aluminum the molecular dynamics simulation [10] shows the upper limit of uniaxially compressed crystal at stresses $\approx 0.4K$, where K is a bulk modulus.

SWs are used for defining of shock Hugoniot and thermodynamic equation of state (EOS) [1, 11–13]. Colliding plates and nanosecond (ns) lasers now are routinely applied for generation of SW [11, 12]. There are recent experiments on laser shock generation based on femtosecond (fs) [2, 3] and subnanosecond (sub-ns) [5, 6] pulses. They open new direction in physics of SW. Simulations [2, 4, 9, 10] allow to understand the internal events caused by fs and sub-ns pulses inside the irradiated target and to demonstrate a superelastic nature of a generated SW (calculation results on sub-ns case remain unpublished). Experiments [2, 3, 5, 6] and simulations [2, 4, 9, 10] (i) reveal that uniaxially compressed lattice survives under huge stresses, (ii) describe elastic branches [1] of Hugoniot adiabats at high volume compressions and pressures, and (iii) discover the dynamic coupling of elastic and plastic SW [10]. This interaction supports propagation of an elastic SW ahead very strong plastic one.

The main advantages of laser-induced shock-wave experiments [2,3,5,6] are (i) synchronization between a pump pulse driving SW and probe pulse following dynamics of expansion of a rear-side surface after arrival of SW; and (ii) high temporal resolution of probing. This resolution is ~ 0.1 ps for fs device [2, 3] and few ps for sub-ns devices [5, 6]. It overcomes by 3-4 orders of magnitudes the resolution of both the velocity interferometer system for any reflector (VISAR) and the optically recording velocity interferometer system (ORVIS). Namely this ultrahigh resolution elucidates a fine structure of combining elastic and plastic SW. Short propagation distance, well defined temporal synchronization of pump and diagnostics, and high temporal resolution allow to observe powerful $p \sim 10$ GPa pure elastic (no accompanying plastic SW) SW in experiments [2, 3, 5, 6]. From the other hand, the pure elastic SW with stress ~ 10 GPa observed in the thicker foils ≈ 10 microns in [5, 14][2] are near the upper limit of the temporal resolution of VISAR and ORVIS. This means that in experiments with foils thicker than 10 microns the powerful elastic jumps can be observed with the help of VISAR/ORVIS in near future.

2. Model and equations

Energy balance for whole electron and ion (e+i) system is separated into two independent energy equations in our 2T condition $T_e > T_i$ in comparison with one-temperature (1T) condition $T_e = T_i = T$. 2T equations gradually transfer into 1T equations inside the same 2T hydrodynamics (2T-HD) code as 2T electron-ion equilibration proceeds in time. In 2T-HD the mass and momentum balances are added to energy equations and additional terms ($p_e u_x$, $p_i u_x$ work on expansion, here $u_x \equiv \partial u/\partial x$) are included into equations for energy. We add elasticity conditions corresponding to isotropic elastic solids into equations of 2T-HD and obtain new code 2T-HD-Elast. Volume density of elastic energy $\tau_{ij}\chi_{ij}/2$ of uniaxial compression for this model of solid is $(K + 4G/3)[\delta(\Delta x)/(\Delta x)]^2/2$ according to Hooke's law; here Δx is thickness of solid layer before deformation, $\delta(\Delta x)/(\Delta x) = \delta\rho/\rho = \chi_{11} = \chi_{xx}$ is relative deformation in direction x of uniaxial motion, τ_{ij}, χ_{ij} are tensor components of stress and deformation. Shear modulus G is an appreciable fraction of bulk modulus K, therefore elastic speed of sound $c_{el} = \sqrt{(K + 4G/3)/\rho}$ is significantly larger than bulk speed of sound $c_{pl} = \sqrt{K/\rho}$; e.g., for aluminum and nickel those parameters are: $K, G\,[\mathrm{GPa}], c_{el}, c_{pl}\,[\mathrm{km/s}] = (76, 26, 6.4, 5.3)$ for Al and $(180, 76, 5.3, 4.5)$ for Ni. The 2T-HD-Elast code differs from 2T-HD by momentum equation:

$$\rho_o \partial u/\partial t = -\partial p_{xx}/\partial x_o, \qquad p_{xx} = p_e + p_i - s_{xx}, \qquad s_{xx} = (4G/3)\partial(x - x_o)/\partial x_o,$$

[1] Each lattice orientation relative to shock direction has its own elastic Hugoniot.

[2] [9] is devoted to prove that in [14] a pure elastic SW has been observed after propagation of a long distance near 10 microns. In [14] only SW velocity D has been measured from the sequence of time instants of breakthrough of SW through the foils of different thicknesses. Piston velocity was not measured in this experiment.

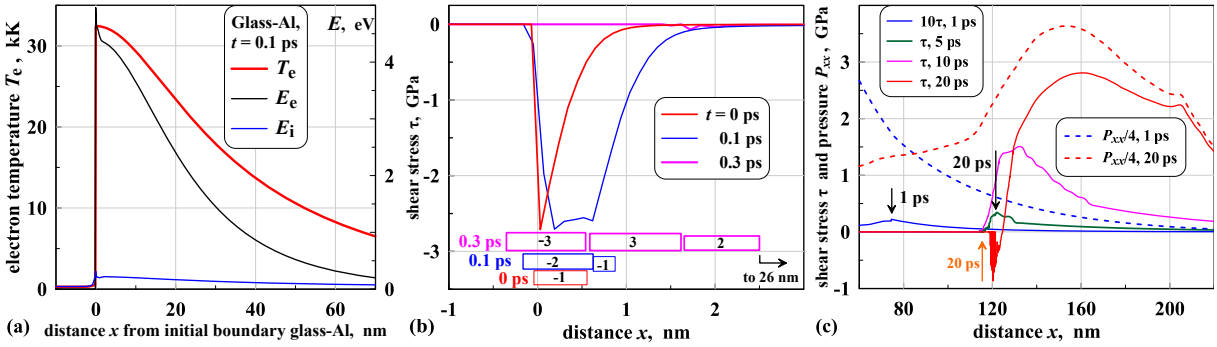

Figure 1. (a) Temperature and energy distributions near the end of heating by a uslP when maximum values of electron thermodynamics parameters are achieved. (b) Heating of lattice by an electron-ion energy transfer, expansion of Al crystal in direction of glass, appearance of negative shear stress (when longitudinal stress p_{xx} is less than transverse stress $p_\perp$), melting of solid, and disappearance of shear. (c) Passing of compression wave from molten to solid aluminum, see also [15]. Black arrows mark positions of solidus at instants 1 and 20 ps, while an orange arrow shows liquidus at $t = 20$ ps. We see how strongly the width of two-phase liquid-solid layer shrinks with time. The inversion of shear stress sign on profile $t = 20$ ps takes place in hot crystal nearby liquid-solid interface, where specific condition of $p_{xx} < p_\perp$ is produced after exit of a maximum of compression wave from the molten layer, see details in text.

where ρ_o, x_o, x are initial density, Lagrangian and Euler coordinates, respectively; p_{xx} and s_{xx} are longitudinal and deviatoric stresses. We suppose that a shear modulus smoothly disappears proportionally to volume fraction of solid in two-phase solid-to-liquid transition layer between molten metal and crystal.

3. Shear stress in solid prior to its melting at 2T stage and propagation of compression wave from liquid to solid

Figure 1 presents simulation by 2T-HD-Elast code of action of ultrashort laser pulse (uslP) onto aluminum film deposited onto glass substrate. UslP parameters are: duration $\tau_L = 100$ fs, absorbed energy $F_{abs} = 0.13$ J/cm^2, skin-depth 15 nm. Time is reckoned from a maximum of Gaussian heating uslP; $x = 0$ corresponds to the initial position of a glass-Al contact. Prior to uslP a glass window is placed at the left side $x < 0$. The contact moves to the left side during motion initiated by laser heating. Glass is supposed to be nonconductive, acoustic impedance Z of Al is slightly above value Z for glass. We neglect this difference and use a wide-range plastic EOS [16, 17] for Al to describe glass. At an early 2T stage all absorbed energy in metal is deposited into electron internal energy E_e, see figure 1(a). Cohesion energy for Al is ≈ 3 eV/atom. At an early stage the energy E_e overcomes this value. But fast (supersonic) conductive redistribution of energy decreases local thermal load down from the values significantly above a critical point to the values of the order of few heats of fusion.

Figure 1(b) illustrates processes of stretching of elastic Al due to expansion in glass, formation of negative shear stress, and unloading of shear as result of melting. Three instants are shown. Finite time interval is necessary for heating of ion subsystem above melting temperature corresponding to current local pressure. During this interval a hot solid near the glass-Al contact is uniaxially stretched in direction to glass mainly by electron pressure p_e. As a result a negative shear stress appears. Digits in figure 1(b) mean: 1, 2, 3 are solid, solid-liquid, liquid stable phases; -1, -2, -3 are metastable stretched solid, solid-liquid, liquid phases. Lengths of rectangles correspond to thickness of the designated phases at the particular instant. During

the time interval $0 \to 0.3$ ps a thin layer of stretched crystal "-1" appears first, after that a stretched liquid-solid layer appears (it coexists with stretched solid), and after that crystal melts and shear drops to zero. At instant $t = 0.3$ ps the stretched and compressed pure liquids contact at the right side with a thick layer of compressed solid-liquid mixture. The layer of this mixture is bound from the left side by liquidus and from the right side by solidus. The point $x = 26$ nm at $t = 0.3$ ps corresponds to the instant position of a solidus. There is some compression of metal near the solidus at $t = 0.3$ ps. It causes formation of positive stress τ. But electronic heat transport is supersonic at an early 2T stage, therefore degree of compression is small, and absolute values of those positive stresses are negligibly small since they are proportional to compression degree.

Thermal transport passes hypersonic, transonic, and subsonic stages during a time interval shown in figure 1(c). Mach number of shift velocity of a point of liquidus decreases from ≈ 5 to ≈ 0.02 at this interval. Much latter at temporal scale 0.1-1 ns the recrystallization solidifies molten layer if aluminum film is significantly thicker than a thermal depth $d_T \approx 100$ nm [18]. Transonic transition lasts from 4 to 6 ps. This is a stage when mainly thermal evolution transfers to mainly mechanical evolution. Profiles of ion thermodynamic parameters T_i, E_i, p_i have kinks [15, 19]. Before the transition those kinks "sit" at the points of solidus and liquidus. But after transonic transition thermodynamic kinks separates from dynamic ones: kinks at the profiles of T_i, E_i remain at the solidus and liquidus, while the kinks at the pressure profiles separates from the points of solidus and liquidus. This is a process of irradiation of compression wave by a sharply decelerating thermal wave. The kinks at the pressure profiles are an "images" of the solidus and liquidus. They move along acoustic characteristics propagating into bulk. Trace of fast melting is seen as more steep piece of profile between acoustic images of solidus and liquidus, see example in figure 1(c) with p_{xx} and τ profiles for $t = 20$ ps. Ratio of pressure to bulk modulus $\approx 15\%$ is not an infinitesimal value. We have weakly nonlinear acoustic wave. Steepness of a wave gradually increases during propagation, see the next section.

There is interesting dynamic interaction between molten Al and solid. There is a steep change (like a jump) of a shear stress $\tau = (p_{xx} - p_\perp)/2$ across the melting front; $\tau = 0$ in liquid, see figures 1(c) and 2. This means that a transverse stress $p_\perp = (p_{yy} + p_{zz})/2$ has steep decrease here because the longitudinal stress p_{xx} is continuous through the melting front. Stress $p_\perp$ is higher than p_{xx} in a crystal layer attached to the melting front. Dynamic coupling of melt and solid can be unstable against plastic instability releasing shear-stress jump in uniaxially compressed solid near the contact. The similar plastic instability in a rarefaction elastic wave has been observed at a boundary between vacuum (where $p_\perp = 0$) and uniaxially compressed solid (where $p_\perp > 0$) in [20, 21]. Decrease of shear-stress jump and widening of transition layer act as stabilizing factors. Irradiation of dislocation from a melting front above some threshold for uniaxial stress p_{xx} has been observed in [15].

Comparison of 2T-HD-Elast and MD is shown in figure 2(a); compare also figures 2(b) and 2(c). Elastic solid (no plastic transformations) begins to the right side from the point of solidus. Hooke's law written for an isotropic elastic solid relates the longitudinal stress $p_{xx} = (K + 4G/3)\chi_{xx}$ to the transverse one $p_{yy} = p_{zz} = p_\perp = (K - 2G/3)\chi_{xx}$ for uniaxial deformation, where $\chi_{yy} = \chi_{zz} = 0$. Then, the shear stress is $\tau = G\chi_{xx}$ from the definition of τ. Let's note that we use $\chi_{xx} = \delta\rho/\rho_o$ with ρ_o corresponding to the initial (room temperature) density of homogeneous Al film. Comparison of stresses according to Hooke's law and simulated ones is shown in figures 2(b, c).

In both 2T-HD-Elast and MD profiles in figures 2(b, c) a surprising phenomenon is seen. Gradually the notable *negative*(!) shear stress τ develops in a visible layer near melting front, see figures 2(b, c). Thus, distribution of τ changes sign near a melting front (shear-stress inversion takes place). What are the reasons for such behavior (inversion of τ)? The reasons are simple. They are connected with heating and rarefaction. For material under uniaxial

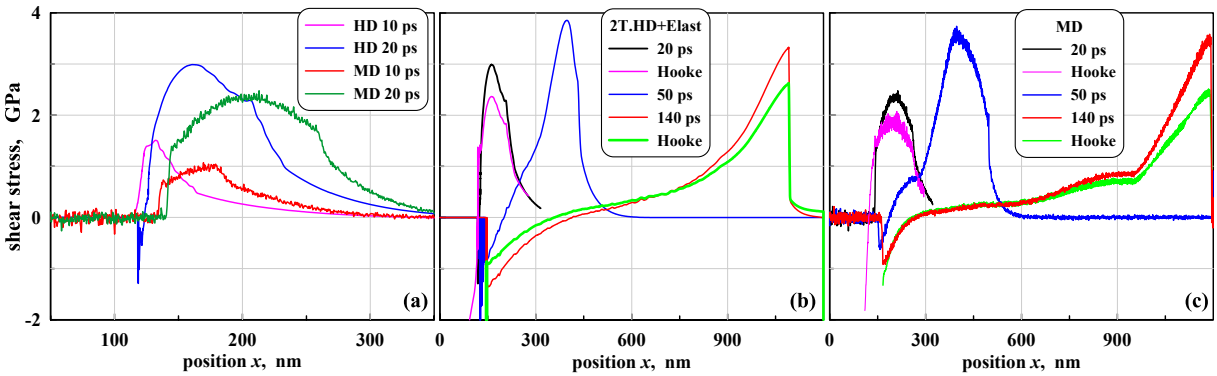

Figure 2. (a) 2T-HD-Elast versus MD. Single fcc Al crystal expanded along direction 111 has been considered in this MD simulation. Both codes show existence of a more steep piece ($x \approx 250$ nm, $t = 20$ ps - trace of fast melting) on a stress profile. Later this piece causes early overturning of elastic compression wave and formation of elastic shock. The elastic shock has an amplitude approximately equal to pressure corresponding to isochoric melting. (b) Evolution of elastic stress in 2T-HD-Elast: propagation through melting front, overturning, amplitude increase, and attenuation. (c) The same evolution in MD. Shock arrives at a rear-side Al-vacuum boundary of Al film 1.2 microns thick at $t \approx 140$ ps.

compression $p_{xx} > p_\perp$ and $\tau > 0$ because $\rho > \rho_o$. But in stretched state $\rho < \rho_o$ and $p_{xx} < p_\perp$, which leads to $\tau < 0$. In the rarefaction tail (to the left side from the pressure maximum in figures 2) the stress p_{xx} is positive. Why then τ becomes negative in a hot layer attached to the melting front? This is because the heating of crystal shifts an equilibrium density for which $p_{ij} \equiv 0$ (the density ρ_o corresponds to room temperature). The heating of crystal with density $\rho = \rho_o$ increases evenly both stresses $p_{xx} = p_\perp$. Therefore, $p_{xx} < p_\perp$ and $\tau < 0$ are produced in the heated crystal layer, which is attached to the melting front, during unloading started after the compression maximum passes through this layer, even though $p_{xx} > 0$ is there.

4. Overturning and subsequent increase and attenuation of elastic stress jump

As was said, nonlinear wave overturns (breaking of Riemann wave). This is effect of nonlinearity - in more compressed piece of a wave the velocity $c + u$ of characteristics is larger than in a less compressed piece. Values p, c, u are conserved along characteristics, therefore the characteristics carrying larger p, c, u overtakes the characteristics with smaller p, c, u. Let at an instant t_1 a velocity profile has a slope u_x. Then a time interval to a breaking is $t_1 - t_{br} \sim 1/u_x$. This means that a more steep piece overturns earlier. The slope at an interval between images of solidus and liquidus in figure 2(a) is twice larger than a slope at the neighbor pieces. Shock appears in a time interval 20–50 ps for considered absorbed laser energy 130 mJ/cm^2. From distribution of a shear stress τ we see that a solid to the right of a molten layer remains in elastically compressed state (no plasticity) in spite of large values of $\tau \approx G/6.5$ [2–4, 9].

Supersonic elastic shock overtakes an acoustic signal emitted from a nose of heated layer; see Figures 2(b, c). While a subsonic flux flowing from the shock behind it can not prevent back side (relative to shock) characteristics to arrive to a shock front. Thus an amplitude of a shock in the first instance increases since a maximum of a pressure profile comes to a front. After that an attenuation of elastic shock begins. It is slightly larger in a 2T-HD-Elast code. This attenuation is mainly caused by rarefaction and divergence of characteristics in a tail part of a wave. Dissipative processes seems are less important in elastically compressed media.

5. Conclusion

An advanced hydrocode 2T-HD-Elast, which combines 2T processes together with an elastic response of crystal to ultrashort laser heating, is developed. Comparison of 2T-HD-Elast modeling with MD simulation confirms that 2T-HD-Elast reproduces well generation and propagation of non-linear elastic waves in metals. 2T elastic behavior of metal prior its melting is studied. Such an effect is dynamically minor but qualitatively significant. Propagation of compression wave from molten to solid layer through the liquid-solid interface is studied in details. An interesting phenomenon of shear-stress inversion near a melt/solid boundary is found. Nonlinear evolution of elastic compression wave transforming into powerful purely elastic shock is investigated. It is tracked how characteristics take out the trace of supersonic melting into elastic shock.

Acknowledgments

Support from RFBR is acknowledged (S.I.A., N.A.I., V.A.Kh. grant 13-02-01078; K.V.Kh. grants 11-08-01225, 13-02-91057, 13-08-12248). V.V.Z was supported by the NSF through grant No. DMR-1008676. MD simulations were performed using NSF XSEDE facilities and the USF Research Computing Cluster.

References

[1] Asay J R and Shahinpoor M (eds) 1993 *High pressure shock compression of solids* (Springer)
[2] Agranat M, Anisimov S, Ashitkov S, Zhakhovskii V, Inogamov N, Komarov P, Ovchinnikov A, Fortov V, Khokhlov V and Shepelev V 2010 *JETP Lett.* **91** 471–477
[3] Ashitkov S, Agranat M, Kanel' G, Komarov P and Fortov V 2010 *JETP Lett.* **92** 516–520
[4] Zhakhovskii V V and Inogamov N A 2010 *JETP Lett.* **92** 521–526
[5] Whitley V H, McGrane S D, Eakins D E, Bolme C A, Moore D S and Bingert J F 2011 *J. Appl. Phys.* **109** 013505
[6] Crowhurst J C, Armstrong M R, Knight K B, Zaug J M and Behymer E M 2011 *Phys. Rev. Lett.* **107**(14) 144302
[7] Evans R et al. 1996 *Phys. Rev. Lett.* **77** 3359–3362
[8] Gahagan K T, Moore D S, Funk D J, Rabie R L, Buelow S J and Nicholson J W 2000 *Phys. Rev. Lett.* **85** 3205–3208
[9] Inogamov N A, Zhakhovskii V V, Khokhlov V A and Shepelev V V 2011 *JETP Lett.* **93** 226–232
[10] Zhakhovsky V V, Budzevich M M, Inogamov N A, Oleynik I I and White C T 2011 *Phys. Rev. Lett.* **107** 135502 (4)
[11] Anisimov S I, Prokhorov A M and Fortov V E 1984 *Sov. Phys. Usp.* **27**
[12] Prokhorov A M, Anisimov S I and Pashinin P P 1976 *Sov. Phys. Usp.* **19** 547–560
[13] Kanel G I, Fortov V E and Razorenov S V 2007 *Phys. Usp.* **50** 771
[14] Huang L, Yang Y, Wang Y, Zheng Z and Su W 2009 *J. Phys.* D **42** 045502
[15] Demaske B J, Zhakhovsky V V, Inogamov N A and Oleynik I I 2013 *Phys. Rev.* B **87** 054109 1–9
[16] Bushman A V, Kanel' G I, Ni A L and Fortov V E 1993 *Intense dynamic loading of condensed matter* (Taylor & Francis)
[17] Shock wave database: http://teos.ficp.ac.ru/rusbank/
[18] Ashitkov S, Inogamov N, Zhakhovsky V, Emirov Y, Agranat M, Oleinik I, Anisimov S and Fortov V 2012 *JETP Lett.* **95** 176–181
[19] Inogamov N et al. 2011 *Contrib. Plasm. Phys.* **51** 367–374
[20] Anisimov S I, Zhakhovskii V V, Inogamov N A, Nishihara K, Oparin A M and Petrov Y V 2003 *JETP Lett.* **77** 606–610
[21] Anisimov S I, Zhakhovskii V V, Inogamov N A, Nishihara K and Petrov Y V 2007 *Appl. Surf. Sci.* **253** 6390–6393